ISSN 0023-1584, Kinetics and Catalysis, 2006, Vol. 47, No. 6, pp. 825–833. © MAIK "Nauka/Interperiodica" (Russia), 2006.
Original Russian Text © A.N. Ermakov, I.K. Larin, A.A. Ugarov, A.P. Purmal, 2006, published in Kinetika i Kataliz, 2006, Vol. 47, No. 6, pp. 849–858.

Size Effects in the Catalysis of Atmospheric Oxidation of SO_2 by Iron Ions

A. N. Ermakov[a], I. K. Larin[a], A. A. Ugarov[a], and A. P. Purmal[b]

[a] *Institute of Energy Problems of Chemical Physics, Russian Academy of Sciences, Chernogolovka, Moscow oblast, 142432 Russia*

[b] *Semenov Institute of Chemical Physics, Russian Academy of Sciences, Moscow, 117977 Russia*

e-mail: ayermakov@chph.ras.ru

Received July 5, 2005

Abstract—The oxidation of SO_2 catalyzed by iron ions in cloud drops of various sizes is analyzed in terms of the reduced model of atmospheric processes. It is demonstrated for the first time that iron ions exert a catalytic effect only in the smallest (<5 μm) and the largest (>100 μm) drops. This behavior of iron ions is due to the variation of the concentration ratio between the active form Fe(III) and the inactive form Fe(II) in the drops. SO_2 oxidation in drops of intermediate sizes is slower, because most of the iron in these drops is in the Fe(II) state.

DOI: 10.1134/S0023158406060036

The liquid-phase oxidation of $SO_{2(g)}$ catalyzed by transition-metal ions is still among the poorly understood heterogeneous chemical processes occurring in the lower atmosphere [1–3]. Not long ago, gaining a deeper insight into this process was impeded by the inadequate understanding of the mechanisms of relevant catalytic reactions [4]. It was only in recent years that catalysis by iron ions[1] was demonstrated to be a chain process with degenerate chain branching [5]. This provided an explanation for the fact that this process is steady-state. An interpretation was also suggested for the earlier unexplained fact that the oxidation process is dramatically accelerated by $S_2O_{8(aq)}^{2-}$ [6], an ion inert towards sulfite, and by Mn_{aq}^{2+}, a catalytically inactive ion (the Fe–Mn ion couple shows so-called synergism [7–10]). These kinetic features of liquid-phase $SO_{2(g)}$ oxidation, as well as a number of other ones, are explained in terms of changes in the ratio of the concentration of the active iron form Fe(III) to the concentration of the inactive iron form Fe(II), the quantity determining the rate of the catalytic reaction [5]. Furthermore, unexpected effects were revealed by simulating iron-ion-catalyzed $SO_{2(g)}$ oxidation in atmospheric water drops [11]. It was found that the turnover frequency of iron ions is ~800 times higher in micron-sized water drops than in vitro under the same concentration conditions. The purpose of this study is to analyze the catalytic oxidation of sulfite in cloud drops of various sizes. Our analysis will be based on the reduced model (RM), which was developed earlier and was used in our previous paper on this subject [21].

Fe(III)/Fe(II) Ion Distribution in Water Drops

In the analysis of the drop-size (r_0) effect on the rate of iron-ion-catalyzed sulfite oxidation, we considered the reactions presented in our previous article [21, Tables 2–4] and the reactions listed in Tables 1–3. The total iron content [Fe(II)] + [Fe(III)] = $[Fe]_0$ was taken to be 10^{-7} mol/l, unless otherwise stated. The other conditions were the same as in the calculations concerning the formation of the oxidizing properties of cloud drops in the absence of iron ions [21].[2] Figure 1 shows an example of the drop-size dependence of iron ion distribution between the Fe(II) and Fe(III) states as

[1] Iron is the most abundant transition metal. The iron abundance in the Earth's crust is 5.6×10^4 ppm [12]. It is due to this fact, along with the low value of the Fe(III)/Fe(II) redox potential ($E^0_{Fe(III)/Fe(II)} = 0.77$ V), that iron is involved in a wide variety of chemical processes in the hydrosphere [14–16] and in atmospheric water drops [3]. The natural and anthropogenic sources of atmospheric iron are coal weathering and combustion [17]. The subsequent dry precipitation of iron as a component of aerosols and rain is considered to be a significant source of oceanic iron [18]. The iron ions present in seawater determine the state of the biota and phytoplankton and thus influence the productivity of the ocean [19, 20].

[2] The nonuniformity of the distribution of the species family $HO^{\cdot}_{2(aq)}/O^{-\cdot}_{2(aq)}$ in the drop, caused by the reactions $HO^{\cdot}_{2(aq)}$ + $HO^{\cdot}_{2(aq)}/O^{-\cdot}_{2(aq)}$ (1A, 2A), $HO^{\cdot}_{2(aq)}/O^{-\cdot}_{2(aq)}$ + $SO_5^{-\cdot}$ (17A, 18A), and $O^{-\cdot}_{2(aq)}$ + Fe(III) (26A, 27A) (see Table 2), was ignored. No analytical solution has been found in the literature for the problem of averaging the concentrations of reactive components diffusing into the drop bulk and participating simultaneously in first- and second-order reactions.

Table 1. Chemical reactions involving iron ions in water drops

Entry	Reaction	$k_{i\mathrm{A}}$, l mol^{-1} s^{-1}
25A	$FeOH^{2+}_{aq} + HO^{\bullet}_{2(aq)} \longrightarrow Fe^{2+}_{aq} + O_{2(aq)} + H_2O$	1.3×10^5
26A	$FeOH^{2+}_{aq} + O^{-\bullet}_{2(aq)} \longrightarrow Fe^{2+}_{aq} + OH^{-}_{aq} + O_{2(aq)}$	1.5×10^8
27A	$Fe(OH)^{2+}_{aq} + O^{-\bullet}_{2(aq)} \longrightarrow Fe^{2+}_{aq} + 2OH^{-}_{aq} + O_{2(aq)}$	1.5×10^8
28A	$Fe^{2+}_{aq} + H_2O_{2(aq)} \longrightarrow OH^{\bullet}_{aq} + OH^{-}_{aq} + Fe^{3+}_{aq}$	76
29A	$Fe^{2+}_{aq} + S_2O^{2-}_{8(aq)} \longrightarrow Fe^{3+}_{aq} + SO^{2-}_{4(aq)} + SO^{-\bullet}_{4(aq)}$	12
30A	$Fe^{2+}_{aq} + HSO^{-}_{5(aq)} \longrightarrow Fe^{3+}_{aq} + SO^{-\bullet}_{4(aq)} + OH^{-}_{aq}$	3.0×10^4
31A	$Fe^{2+}_{aq} + O^{-\bullet}_{2(aq)} \xrightarrow{2H^+} H_2O_{2(aq)} + Fe^{3+}_{aq}$	1.0×10^7
32A	$Fe^{2+}_{aq} + HO^{\bullet}_{2(aq)} \longrightarrow Fe^{3+}_{aq} + HO^{-}_{2(aq)}$	1.2×10^6
33A	$Fe^{2+}_{aq} + SO^{-\bullet}_{4(aq)} \longrightarrow Fe^{3+}_{aq} + SO^{2-}_{4(aq)}$	3.0×10^8
34A	$Fe^{2+}_{aq} + SO^{-\bullet}_{5(aq)} \longrightarrow Fe^{3+}_{aq} + SO^{2-}_{5(aq)}$	3.2×10^6
35A*	$FeOHSO_3H^{+}_{aq} \longrightarrow Fe^{2+}_{aq} + H_2O + SO^{-\bullet}_{3(aq)}$	0.2

* The rate constant has dimensions of s^{-1}.

$\zeta = ([Fe(III)]/[Fe(II)])$ ($t_{ex} = 5 \times 10^3$ s). Curve *1* reflects the overall effect of the *S*/*V* factor and of the nonuniformity of the $OH^{\bullet}_{aq}$ and $O_{3(aq)}$ in the drop, while curve *2* illustrates only the effect of *S*/*V*. The fact that the curves do not coincide suggests that the nonuniformity of the distribution of the above species, particularly $OH^{\bullet}_{aq}$, has a strong effect on the Fe(III)-to-Fe(II) concentration ratio. The time factor in the distribution of iron between its valence states is illustrated by the time variation of $\zeta_t = ([Fe(III)]/[Fe(II)])_t$ calculated for micron-sized drops (Fig. 2). Figure 2 shows the corresponding plots of $[S(IV)]_t$ and pH_t for these drops. In spite of the considerable extent of gas self-cleaning of $SO_{2(g)}$ ($[S(IV)]_{t=0}/[S(IV)]_{t=10^4\ s} \approx 3$) and the marked increase in the acidity of the drops ($\Delta pH \approx -0.5$), the changes in $[S(IV)]_t$ and pH_t do not cause any redistribution of iron between its valence states, even though they affect ζ. At long exposure times, the oxidized form Fe(III) remains the dominant iron species in micron-sized drops. As for the drop size effect, drop growth causes a redistribution of iron between its valence states. The drop size effect shows a kind of zonal variation (see the hatched regions in Fig. 1). The oxidized form of iron ions dominates only in the smallest (≤5 μm) and largest (≥100 μm) drops. The drops of intermediate sizes are dominated by the reduced form of iron. Our calculations have demonstrated that the distribution of iron ions between the Fe(II) and Fe(III) states depends on $[Fe]_0$. As $[Fe]_0$ is raised in submicron-sized drops, ζ changes in favor of Fe(III). For example, $\zeta_{r_0 = 1\ \mu m} \approx 9$ for $[Fe]_0 = 4 \times 10^{-7}$ mol/l. This deduction is not in conflict with the results of our previous study [22], where a value of $\zeta_{r_0 = 1\ \mu m} \approx 1$ was reported for similar conditions ($[SO_{2(g)}] = 1$ ppb, $[Fe]_0 = 5 \times 10^{-7}$ mol/l, $L = 3 \times 10^{-7}$; calculations using the CAPRAM 2.3 model). Note that, as distinct from RM, CAPRAM 2.3 takes into consideration the liquid-phase oxidation of $HCOO^{\bullet}_{aq}/HCOO^{-}_{aq}$, $CH_2(OH)_{2(aq)}$, and a number of other organic compounds and the fast reactions $OH^{\bullet}_{aq}/O^{-\bullet}_{2aq}$ + Cu^{2+}/Cu^{+} and Fe(III) + Cu^{+}. As demonstrated in our earlier work [21], up to ~50% of the $OH^{\bullet}_{g}$ species entrained from the gas are consumed in reactions involving $HCOOH_{aq}/HCOO^{-}_{aq}$ and $CH_2(OH)_{2(aq)}$. However, it was demonstrated in an independent study [23] that radical acceptors, such as benzene, weaken the oxidizing capacity of sulfite solutions towards the Fe(III)/Fe(II) ion couple. At $[Fe]_0 = 10^{-5}$ mol/l, $[S(IV)] \approx 2 \times 10^{-3}$ mol/l, and pH ≈ 3, the ratio of the oxidized and reduced iron forms decreases by a factor of about 2 both in the presence and in the absence of ben-

Table 2. Photodissociation processes in the liquid phase

Entry	Process	$J_{i\mathrm{A}}$, s^{-1}
39A	$FeOH^{2+}_{aq} \xrightarrow{h\nu} Fe^{2+}_{aq} + OH^{\bullet}_{aq}$	4.5×10^{-3}
40A	$Fe(OH)^{+}_{2(aq)} \xrightarrow{h\nu} Fe^{2+}_{aq} + OH^{\bullet}_{aq} + OH^{-}_{aq}$	5.8×10^{-3}
41A	$FeSO^{+}_{4(aq)} \xrightarrow{h\nu} Fe^{2+}_{aq} + SO^{-\bullet}_{4(aq)}$	1×10^{-4}

Note: $J_{i\mathrm{A}}$ is the photodissociation coefficient.

Table 3. Hydrolysis and complex formation equilibria in water drops

Entry	Equilibrium	K_{iE}, l/mol	Forward reaction	Reverse reaction
			$\vec{A}_{298}$, $\frac{l^{-(n-1)}}{mol^{-(n-1)}\,s}$	$\overleftarrow{A}_{298}$, $\frac{l^{-(n-1)}}{mol^{-(n-1)}\,s}$
14E	$FeOH^{2+}_{aq} + HSO^{3-}_{3(aq)} \rightleftharpoons FeOHSO_3H^{+}_{aq}$	600	5.0×10^{10}	8.3×10^{7}
15E	$FeOH^{2+}_{aq} + SO^{2-}_{3(aq)} \rightleftharpoons FeOHSO_{3(aq)}$	2.0×10^{7}	5.0×10^{10}	2.5×10^{3}
16E*	$FeOH^{2+}_{aq} + H_2O \rightleftharpoons Fe(OH)^{2+}_{aq} + H^{+}_{aq}$	7.0×10^{-5}	5.6×10^{5}	8.0×10^{9}
17E	$Fe^{2+}_{aq} + SO^{2-}_{4(aq)} \rightleftharpoons FeSO_{4(aq)}$	158	7.9×10^{12}	5.0×10^{10}
18E	$Fe^{3+}_{aq} + HSO^{-}_{3(aq)} \rightleftharpoons FeHSO^{2+}_{3(aq)}$	72	5.0×10^{10}	6.9×10^{8}
19E	$Fe^{3+}_{aq} + SO^{2-}_{3(aq)} \rightleftharpoons FeSO^{+}_{3(aq)}$	7.3×10^{6}	5.0×10^{10}	6850
20E	$Fe^{3+}_{aq} + SO^{2-}_{4(aq)} \rightleftharpoons FeSO^{+}_{4(aq)}$	180	3.2×10^{7}	1.8×10^{5}
21E*	$Fe^{3+}_{aq} + H_2O \rightleftharpoons FeOH^{2+}_{aq} + H^{+}_{aq}$	2×10^{-3}	8.6×10^{5}	4.3×10^{8}

Note: K_{iE} is the equilibrium constant, n is the order of the reaction, $\vec{A}_{298}$ is the preexponential factor at 298 K for the forward reaction, $\vec{E}_a$ is the activation energy of the forward reaction, and $\overleftarrow{A}_{298}$ is the exponential factor at 298 K for the reverse reaction.
* The equilibrium constant is dimensionless.

zene (~10^{-3} mol/l). The drops with $r_0 = 10$ μm are dominated by Fe^{2+} in the daytime even at a much higher iron concentration of $[Fe]_0 = 5 \times 10^{-6}$ mol/l ($L = 3 \times 10^{-7}$, $\zeta_{r_0 = 10\ \mu m} \approx 0.2$) [24]. In the study cited (in which the M2C2 model was used), as in the study by Herrmann et al. [22], the liquid-phase oxidation of $HCOOH_{aq}/HCOO^{-}_{aq}$ and $CH_2(OH)_{2(aq)}$ and processes involving copper ions were taken into consideration along with reactions involving iron ions.

Figure 3 plots the calculated average $\overline{OH^{\cdot}_{aq}}$ and $\overline{HO^{\cdot}_{2(aq)}}$ concentrations (i.e., $[\overline{OH^{\cdot}_{aq}}]_{Fe}$ and $[\overline{HO^{\cdot}_{2(aq)}}]_{Fe}$ ($[\overline{HO^{\cdot}_{2(aq)}}]_{Fe} + [\overline{O^{-\cdot}_{2(aq)}}]_{Fe}$)) as a function of the drop size. For comparison, we demonstrate the effect of drop growth on $[\overline{OH^{\cdot}_{aq}}]$ and $[\overline{HO^{\cdot}_{2(aq)}}]$ in the absence of iron ions (dotted curves). Clearly, iron ions cause nonmonotonicity in $[\overline{OH^{\cdot}_{aq}}]_{Fe} = f(r_0)$. Note that, as the drop

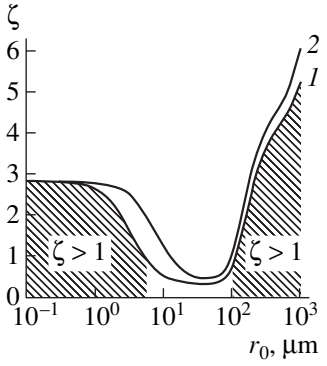

Fig. 1. Drop size effect on the ratio of the valence forms of iron ions in a tropospheric cloud calculated having regard to (*1*) both the *S*/*V* factor and the nonuniform $OH^{\cdot}_{aq}$ and $O_{3(aq)}$ distributions in the drop and (*2*) the *S*/*V* factor alone. Conditions: daytime, $L = 10^{-6}$, $[Fe]_0 = 10^{-7}$ mol/l, and $t_{ex} = 5 \times 10^{3}$ s.

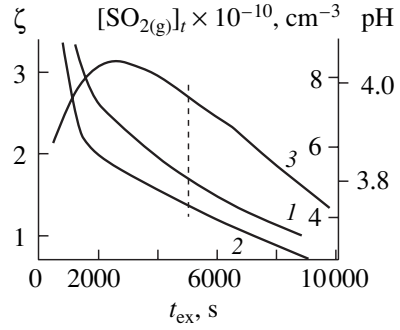

Fig. 2. Time dependence of (*1*) pH in the drop, (*2*) SO_2 concentration (including the species dissolved in the drop), and (*3*) ζ. $r_0 = 1$ μm.

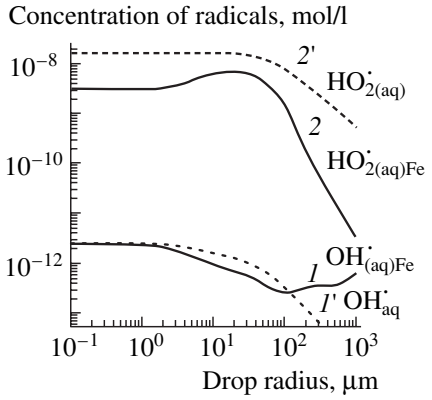

Fig. 3. Drop-size effect on the average concentrations (see main text) of (*1*, *1*') hydroxyl and (*2*, *2*') hydroperoxyl radicals in tropospheric clouds in the (*1*, *2*) presence and (*1*', *2*') absence of iron ions. Conditions: daytime, $L = 10^{-6}$, $[Fe]_0 = 10^{-7}$ mol/l, and $t_{ex} = 5 \times 10^3$ s.

grows, $[\overline{OH_{aq}^{\cdot}}]_{Fe}$ increases in spite of the decreasing influx of these species into the drop. It is evident from Fig. 3 that $[\overline{OH_{aq}^{\cdot}}]_{Fe} \longrightarrow [\overline{OH_{aq}^{\cdot}}]$ for small drops. However, as r_0 increases, the solid and dotted curves diverge more and more widely, with $[\overline{OH_{aq}^{\cdot}}]/[\overline{OH_{aq}^{\cdot}}]_{Fe} > 1$. This divergence between the curves is due to the fact that the decline of $[\overline{OH_{aq}^{\cdot}}]_{Fe}$ begins at a smaller drop size and is more rapid than the decline of $[\overline{OH_{aq}^{\cdot}}]$. According to our calculations, the primary cause of the decrease in the $OH_{aq}^{\cdot}$ concentration in the absence and presence of iron ions is the nonuniformity of the $OH_{aq}^{\cdot}$ distribution in the drop bulk. The apparent strengthening of this factor in the presence of iron ions is due to the bulk generation of hydroxyl radicals via the reaction $O_{2(aq)}^{-\cdot} + O_{3(aq)}$ (10A) being suppressed by the fast reactions (26A) and (27A), in which $O_{2(aq)}^{-\cdot}$ radicals are consumed. This results in a dramatic decrease in the concentration of hydroperoxyl radicals in small drops: $[\overline{HO_{2(aq)}^{\cdot}}]_{Fe}/[\overline{HO_{2(aq)}^{\cdot}}] \ll 1$ (Fig. 3). The negative effect of reactions (26A) and (27A) on the $HO_{2(aq)}^{\cdot}$ concentration is also evident from the fact that $[\overline{HO_{2(aq)}^{\cdot}}]_{Fe}$ and $[\overline{HO_{2(aq)}^{\cdot}}]$ converge as the drop grows. As this takes place, most of the iron ions undergo reduction (Fig. 1) and the negative effect of reactions (26A) and (27A) on the $HO_{2(aq)}^{\cdot}$ concentration weakens. The suppression of reactions (26A) and (27A) resumes the reaction $O_{2(aq)}^{-\cdot} + O_{3(aq)} \xrightarrow{H^+} OH_{aq}^{\cdot}$ (10A). In combination with the increasing rates of photoreactions (39A)–(41A), this ensures the above-noted buildup of $OH_{aq}^{\cdot}$ at $r_0 \geq 100$ μm (Fig. 3). The occurrence of reactions (10A) and (39A)–(41A) in large drops is consistent with the fact that $[\overline{HO_{2(aq)}^{\cdot}}]_{Fe}$ falls more rapidly than the same concentration in the absence of iron ions. This effect is due to reactions (26A) and (27A) coming into play.

As follows from Fig. 1, the growth of the drops causes two inversions in the iron ion distribution between the valence states. This is caused by changes in the oxidation and reductions rates in the Fe(II)/Fe(III) system. In the drops with $r_0 \leq 100$ μm, the reduction of Fe(III) is almost solely due to the reactions involving $HO_{2(aq)}^{\cdot}/O_{2(aq)}^{-\cdot}$ (reactions (26A) and (27A)), while the regeneration of these ions is intimately associated with the conjugate process of $SO_{2(g)}$ oxidation, as is demonstrated by our calculations. Indeed, the direct oxidation $OH_{aq}^{\cdot}$ + Fe(II) cannot play a significant role at low $OH_{aq}^{\cdot}$ and iron ion concentrations ($[Fe]_0 = 10^{-7}$ mol/l). The regeneration of Fe(III) by hydrogen peroxide (reaction (28A)) is also ruled out. All of the $H_2O_{2(g)}$ is exhausted at much earlier stages, at least in the case of small drops. The contribution from $H_2O_{2(aq)}$ synthesized in drops via reactions (1A), (2A), (31A), and (32A) is also insignificant. The real cause is the much more rapid $H_2O_{2(aq)}$ consumption in the reaction involving $HSO_{3(aq)}^{-}$ (3A). Therefore, hydrogen peroxide makes a much smaller contribution to Fe(II) oxidation than the reactions of the $SO_{4-5(aq)}^{-\cdot}$ radical (reactions (33A) and (34A)), whose total rate is, however, no higher than ~10% of the calculated Fe(II) oxidation rate. The main oxidizer of Fe(II) ions is $HSO_{5(aq)}^{-}$, which is an intermediate in the liquid-phase oxidation of sulfur dioxide. The interrelation of these processes under field conditions was reported in, e.g., [25]. Indirect evidence of this interrelation can be found in [26, 27]. A similar result was reported for iron-ion-catalyzed sulfite oxidation under laboratory conditions [28]. While the synthesis of $HSO_{5(aq)}^{-}$ in drops is due to the cross reactions (17A) and (18A), the formation of this species in vitro is due to reactions (19A)–(22A) or reaction (34A) [23]. These considerations provide information concerning not only the Fe(III)/Fe(II) concentration ratio in cloud drops but also the drop-size dependence of this ratio. In the smallest drops, the dynamics of the cyclic process Fe(III) $\rightleftharpoons$ Fe(II) is slowed down by reactions (26A) and (27A). The characteristic time of these reactions in micron-sized drops is estimated at $\tau_{26A}^{*} \approx 10$ s, where $\tau_{26A}^{*} = \tau_{26A}\tau_{27A}/(\tau_{26A} + \tau_{27A})$. Therefore, for $t_{ex} = 5 \times 10^3$ s (Fig. 1), the number of Fe(III)–Fe(II) turnovers is close to 500. However, the deceler-

ating effect of reactions (26A) and (27A) on the cyclic process Fe(III) $\rightleftharpoons$ Fe(II) is disrupted in larger drops (Fig. 1) because of a decrease in the influx of $OH_g^\bullet$ radicals from the gas phase. As a consequence, the rate of the reaction chain $OH_{aq}^\bullet + HSO_{3(aq)}^- \xrightarrow{O_2} HSO_{5(aq)}^-$ (reactions (5A) and (12A)) falls, resulting in a slowdown of the reactions leading to $HSO_{5(aq)}^-$ buildup (reactions (17A) and (18A)). This slowdown decelerates reaction (30A), thus weakening the oxidizing ability of the drops towards both $SO_{2(g)}$ and Fe(II) (conjugate reactions). It is this effect that causes ζ to decrease from ~3 to ~0.3 (Fig. 1). Simultaneously, the $HO_{2(aq)}^\bullet$ concentration increases by a factor of about 3 (Fig. 3) in spite of the decreasing $\vec{\Psi}_{HO_2}$. According to our calculations, this increase is due to the suppression of $O_{2(aq)}^{-\bullet}$ consumption in reactions (26A) and (27A) because of the decrease in [Fe(III)]. By expressing ζ in terms of the concentrations of the oxidizers and reducers of the Fe(III) and Fe(II) ions, we obtain the following formula for the change in ζ upon drop growth from 0.1 to 10 μm:

$$\frac{\zeta_{r_0 = 0.1\ \mu m}}{\zeta_{r_0 = 10\ \mu m}} \approx \frac{[O_2^{-\bullet}]_{r_0 = 0.1\ \mu m}[HSO_{5(aq)}^-]_{r_0 = 0.1\ \mu m}}{[O_2^{-\bullet}]_{r_0 = 10\ \mu m}[HSO_{5(aq)}^-]_{r_0 = 10\ \mu m}}$$

$$\approx 3\frac{[HSO_{5(aq)}^-]_{r_0 = 0.1\ \mu m}}{[HSO_{5(aq)}^-]_{r_0 = 10\ \mu m}}.$$

From these calculations and the data presented in Fig. 1, it follows that $\zeta_{r_0 = 0.1\ \mu m}/\zeta_{r_0 = 10\ \mu m} \approx 10$; hence, $([HSO_{5(aq)}^-]_{r_0 = 0.1\ \mu m}/[HSO_{5(aq)}^-]_{r_0 = 10\ \mu m}) \approx 3$. Thus, the growth of drops within the limits considered might be expected to reduce the $HSO_{5(aq)}^-$ generation rate by a factor of about 3. However, it follows from independent data [29] that, in the absence of an $OH_{aq}^\bullet$ source, $([OH_{aq}^\bullet]_{surf}/\overline{[[OH_{aq}^\bullet]_{Fe}}_{r_0 = 10\ \mu m} \approx 7$ in the drop bulk; that is, the generation rate and, accordingly, the concentration of $HSO_{5(aq)}^-$ is predicted to decrease by a factor of ~7 rather than ~3. The higher $HSO_{5(aq)}^-$ concentration deduced from our calculations indicates that there are sources of these species other than $OH_g^\bullet$ entrainment from the gas phase. These sources cannot be provided by the reaction chain $O_{2(aq)}^{-\bullet} + O_{3(aq)} \xrightarrow[(10A)]{H^+} OH_{aq}^\bullet \xrightarrow[(5A),\ (12A)]{HSO_3^-,\ O_2} SO_{5(aq)}^{-\bullet} \xrightarrow[(17A),\ (18A)]{HO_2/O_2^-} HSO_{5(aq)}^-$ (whether or not iron ions are present). In the presence of iron ions, this chain is terminated by the $O_{2(aq)}^{-\bullet}$ + Fe(III) reactions (26A) and (27A): $w_{10A}/(w_{26A} + w_{27A})_{r_0 = 10\ \mu m} \leq$ 0.14. The photochemical generation of $OH_{aq}^\bullet$ (reaction (37A)) is also of low significance for this drop size (see above). Our calculations have demonstrated that reactions (17A) and (18A) remain the main source of $HSO_{5(aq)}^-$ at $r_0 = 10$ μm. However, as the drop grows, the $SO_{5(aq)}^{-\bullet}$ formation mechanism changes radically. In a large drop, $OH_g^\bullet$ is generated by an iron-ion-catalyzed reaction chain converting $HO_{2(g)}^\bullet$ into $SO_{5(aq)}^{-\bullet}$ [11] along with being entrained from the gas phase. This reaction chain is possible in the atmosphere only due to the conjugation of reactions (26A) and (27A) with the chain branching reaction $Fe_{aq}^{2+} + HSO_{5(aq)}^-$ (30A). The key role in this conjugation is played by the chain branching reaction (30A). Compensating for the loss of Fe(III) ions in reactions (26A) and (27A), the chain branching causes a buildup of $SO_{4(aq)}^{-\bullet}$ species at the same time. Participating in the fast reactions (15A) and (16A) and then in reactions (12A), (17A), and (18A), these species regenerate the peroxomonosulfate consumed in reaction (30A). This conjugation of chemical and photochemical processes depreciates, in part, the results of the model studies of the redox properties of iron ions in cloud water samples under laboratory conditions. For example, Fe(II) formation was observed in the photolysis of filtered aqueous solutions of aerosol particles in the presence of the oxalate ion [30]. However, from these data, it is difficult to derive any conclusion as to the role of the photochemical reduction of iron(III) oxalate complexes in the atmosphere, because this process takes place against the background of the intensive bombardment of the drops with $OH_g^\bullet$ and $HO_{2(g)}^\bullet$.

According to our earlier data [11], the conjugation of reactions (26A) and (27A) with reaction (30A) in the atmosphere can be represented as the following chain of liquid-phase reactions:

$$FeOH_{aq}^{2+} + HO_{2(aq)}^\bullet \longrightarrow Fe_{aq}^{2+} + H_2O + O_{2(aq)},$$

$$Fe_{aq}^{2+} + HSO_{5(aq)}^- \longrightarrow FeOH_{aq}^{2+} + SO_{4(aq)}^{-\bullet},$$

$$SO_{4(aq)}^{-\bullet} + HSO_{3(aq)}^- \longrightarrow SO_{3(aq)}^{-\bullet} + H_{aq}^+ + SO_{4(aq)}^{-\bullet},$$

$$SO_{3(aq)}^{-\bullet} + O_{2(aq)} \longrightarrow SO_{5(aq)}^{-\bullet},$$

$$\overline{HO_{2(aq)}^\bullet + HSO_{3(aq)}^- + HSO_{5(aq)}^-}$$

$$\longrightarrow SO_{4(aq)}^{2-} + H_{aq}^+ + H_2O_{aq} + SO_{5(aq)}^{-\bullet}$$

or $HO_{2(aq)}^\bullet \xrightarrow{Fe} SO_{5(aq)}^{-\bullet}$. It is these processes that make up the extra source of $SO_{5(aq)}^{-\bullet}$, compensating for the loss of this species in the drops "impenetrable" for $OH_{aq}^\bullet$. For the smallest drops such that $q_{OH} < 1$ (the

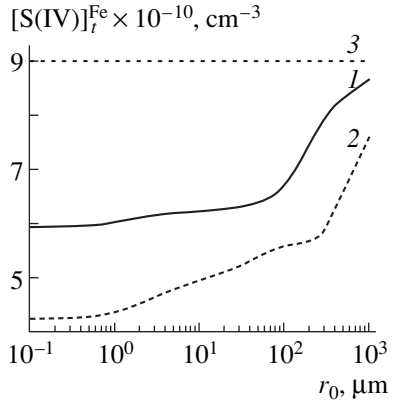

Fig. 4. Drop-size effect on the concentration of unreacted sulfur dioxide ($SO_{2(g)}$ + sulfite in the liquid phase) in the presence of iron ions: (*1*) $t_{ex} = 10^3$ s, (*2*) $t_{ex} = 5 \times 10^3$ s, and (*3*) initial S(IV) concentration ($[S(IV)]_{t=0}$). Conditions: daytime, $L = 10^{-6}$, and $[Fe]_0 = 10^{-7}$ mol/l (see main text).

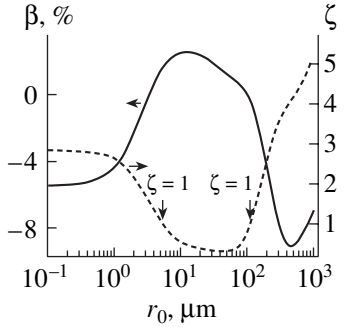

Fig. 5. Size effect in the iron-ion-catalyzed oxidation of $SO_{2(g)}$ in water drops. Conditions: daytime, $L = 10^{-6}$, and $[Fe]_0 = 10^{-7}$ mol/l. The dashed curve represents the drop-size dependence of ζ (see main text).

parameter q is defined in our previous paper [21]), the $SO_{5(aq)}^{-\bullet}$ radicals formed by the catalytic mechanism add to the radicals resulting from the entrainment of $OH_g^\bullet$ from the gas phase. This almost doubles the $SO_{5(aq)}^{-\bullet}$ generation rate relative to the generation rate in the absence of iron ions. The increase in the generation rate of this species causes an increase in the rate of the cross reactions (17A) and (18A). Up to ~60% of the $HSO_{5(aq)}^-$ resulting from these reactions is spent for Fe(II) oxidation. In the drops with r_0 = 10 μm, the increase in the $SO_{5(aq)}^{-\bullet}$ generation rate calculated with neglect of reaction (10A) is as large as ~600% owing to the nonuniform distribution of hydroxyl radicals in the drop bulk. However, the absolute $SO_{5(aq)}^{-\bullet}$ formation rate is obviously lower in these drops than in micron-sized drops. As a consequence, the ratio of the valence states of iron is changed in favor of Fe(II). Therefore, in drops larger than the reaction length for the $OH^\bullet$ radical, the only oxidizer and reducer of the Fe(III)/Fe(II) system are reactions involving $HO_{2(g)}^\bullet$ entrained from the gas phase. The reduction of trivalent iron is due to the fast reactions (26A) and (27A). The oxidation of Fe(II) involving $HO_2^\bullet$ radicals is due to the partial conversion of these radicals into $SO_{5(aq)}^{-\bullet}$ and then $HSO_{5(aq)}^-$. The inference that the ratio of the valence states of the iron ions is determined only by reactions of the $HO_2^\bullet$ radical follows from the fact that ζ remains constant as r_0 is varied between 10 and 60 μm (Fig. 1). This constancy of ζ against the background of the rapidly declining $HO_{2(aq)}^\bullet$ concentration (Fig. 3) is possible only if both the oxidation and the reduction of iron ions is due to reactions involving the same species, in particular, the hydroperoxyl radical (reactions (26A) and (27A)). It is clear from Fig. 1 that the oxidizing capacity of the drops towards Fe(II) is restored only at a drop size of $r_0 \geq 60$ μm. This is due to the above-mentioned reaction (10A) and the photochemical processes (37A) and (39A)–(41A). This follows from the data presented in Fig. 3, which indicate that, although the $OH_g^\bullet$ influx from the gas phase decreases, the $OH_{aq}^\bullet$ concentration increases. In the absence of Fe ions, the $OH_{aq}^\bullet$ concentration only decreases with increasing drop size (Fig. 3, dashed curve *1*).

Catalysis of Atmospheric Sulfite Oxidation by Iron Ions

A detailed analysis of catalytic $SO_{2(g)}$ oxidation in the atmosphere for 1-μm drops was reported in an earlier publication [11]. Below, we will present an analysis of the drop size effect on the dynamics and mechanism of this process. The calculated $[S(IV)]_t^{Fe} = f(r_0)$ curves (Fig. 4), where $[S(IV)]_t = [SO_{2(g)}]_t + [\text{sulfite}]_t N_A L/10^3$, are similar to their counterparts for the noncatalytic process. As in the absence of iron ions, gas self-cleaning of sulfur dioxide proceeds in steps: the first, rapid, step of sulfite oxidation is followed by a slow step. In accordance with earlier data [11], the role of iron ions is more pronounced in the slow step. The effect of iron is most clearly illustrated by Fig. 5. Here, the measure of the involvement of iron ions is $\beta = ([S(IV)]^{Fe}_{t_{ex} = 5 \times 10^3\ s} - [S(IV)]_{t_{ex} = 5 \times 10^3\ s}) \times 100\%/[S(IV)]^{Fe}_{t_{ex} = 5 \times 10^3\ s}$. The plot of this quantity as a function of the drop size is similar to the mirror image of the $\zeta = f(r_0)$ curve (see the dashed curve in Fig. 5). A comparison between these curves leads to the unexpected inference that the iron ions present in cloud drops do not always accelerate the

liquid-phase oxidation of $SO_{2(g)}$. The catalytic effect of these ions depends strongly on the drop size. The catalytic oxidation of $SO_{2(g)}$ is faster than the corresponding noncatalytic process only in drops in which the dominant iron form is Fe(III). In the drops dominated by Fe(II), catalytic $SO_{2(g)}$ oxidation is slower than the noncatalytic process. This deduction is in conflict with experimental data for iron-ion-catalyzed sulfite oxidation in vitro [23]. No matter what the initial state of the iron ions introduced into the sulfite solution, a steady state oxidation regime is established after some time, specifically, the induction period. In this regime, the process rate exceeds the rate of the noncatalytic process and some steady-state distribution of iron between its valence states is observed [23]. The cause of the difference between the catalytic effects of iron ions in the atmosphere and in vitro is obvious. In vitro (in the absence of iron ions), sulfite is stable over an indefinitely long time [31]. In the atmosphere, even if no metal ions are present in the cloud drops, the slow step of $SO_{2(g)}$ oxidation takes place owing to the formation of $H_2O_{2(aq)}$ (reactions (1A) and (2A)) and $HSO_{5(aq)}^-$ (reactions (17A) and (18A)) followed by reactions (3A) and (6A). The effects of the catalytically active, trivalent, iron ions in small and large drops are different. In small drops, the increase in the sulfur dioxide conversion due to iron ions does not exceed ~6%. Obviously, this moderate effect of the iron ions does not imply that the catalytic activity of these ions is low [11]. Sulfite oxidation (reaction (6A)) in iron-containing drops, as opposed to the noncatalytic process, involves only ~40% of the $HSO_{5(aq)}^-$ synthesized; that is, no more than 2×10^6 Fe(III) $\rightleftharpoons$ Fe(II) turnovers per second take place in 1 cm^3 of the gas. Most of the $HSO_{5(aq)}^-$ sustains the steady-state regime of the conjugation of reactions (26A), (27A), and (30A). The accelerating effect of the iron ions is due to reactions (15A) and (16A) [25]. According to our calculations, the contribution from these reactions is as large as 40% of the contribution from reaction (3A), which involves hydrogen peroxide arriving from the gas phase. The participation of iron ions in sulfite consumption is also indicated by the data presented in Fig. 6. Here, $\delta_{S(IV),\,Fe}$ is plotted against the drop size. This plot illustrates the effect of the screening of the $OH_{aq}^{\bullet}$ and $O_{3(aq)}$ fluxes from the gas phase on $SO_{2(g)}$ oxidation. For comparison, Fig. 6 presents data characterizing the drop-size effect on the same parameter in the absence of iron ions ($\delta_{S(IV)}$). In the presence of Fe ions, the adverse effect of the nonuniformity of the $OH_{aq}^{\bullet}$ and $O_{3(aq)}$ distributions in the drop bulk is substantially stronger because of the suppression of reactions (1A), (2A), and (10A). This is the reason why the catalytic activity of iron ions in small drops might appear to be low [11]. Reverting to the variability of the catalytic activity of iron ions (Fig. 4), we can see that the accelerating effect of these ions in

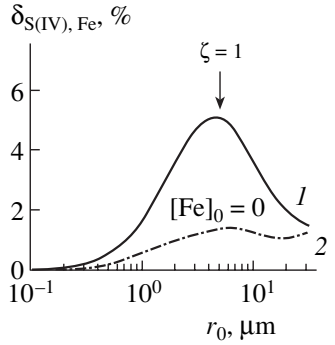

Fig. 6. Plots of (*1*) $\delta_{S(IV),\,Fe}$ and (*2*) $\delta_{S(IV)}$ versus drop radius. Conditions: daytime, $L = 10^{-6}$, and $[Fe]_0 = 10^{-7}$ mol/l (see main text).

$SO_{2(g)}$ oxidation somewhat strengthens as the drop size increases. In the large drops, $SO_{2(g)}$ is primarily consumed by reacting with hydrogen peroxide coming from the gas phase. Hydrogen peroxide oxidizes up to 50% of the sulfite present in the drops. At the same time, as the oxygen oxidation of $SO_{2(g)}$ initiated by the reaction $HO_{2(aq)}^{\bullet} \xrightarrow{Fe} SO_{5(aq)}^{-\bullet}$ declines because of drop growth, reaction (10A) and the photochemical decomposition of Fe(III) hydroxo complexes (reactions (39A) and (40A)) come into play. These hydroxo complexes in the drops serve as photoreceptors. The $OH_{aq}^{\bullet}$ radicals resulting from their photodissociation are converted into sulfite radicals (reactions (5A) and (6A)) and then into $SO_{5(aq)}^{-\bullet}$ radicals (reaction (12A)). The latter participate in the short-chain oxidation of $SO_{2(g)}$ according to the scheme $SO_{5(aq)}^{-\bullet} + SO_{5(aq)}^{-\bullet}$ (reactions (23A) and (24A)). $SO_{2(g)}$ is consumed in the liquid-phase reaction $SO_{4(aq)}^{-\bullet} + HSO_{3(aq)}^-$ (15A). Chain termination in this short-chain process is due to the reactions $SO_{5(aq)}^{-\bullet} + SO_{5(aq)}^{-\bullet} \longrightarrow S_2O_{8(aq)}^{2-} + O_2$, $SO_{4(aq)}^{-\bullet} + Fe_{aq}^{2+}$, and $SO_{5(aq)}^{-\bullet} + Fe_{aq}^{2+}$ (reactions (23A), (33A), and (34A)). According to our calculations, the chain length in sulfite oxidation is approximately five units.

Comparison with Field Data

A number of field studies of the distribution of iron between its valence states in atmospheric water drops have been reported in the literature. For example, $[Fe(II)]/[Fe]_\Sigma \approx 0.2$ for drops of so-called radiation fog in the nighttime.[3] After sunrise, the fraction of Fe(II) ions grows to reach 90% of the total iron content. Furthermore, this fraction depends on the nature of the

[3] Here, $[Fe]_\Sigma$ is the total iron content of the moisture sample, including insoluble iron forms.

aerosol particles. In the aerosol sampled over the sea, $[Fe(II)]/[Fe]_\Sigma \approx 0.5$. The same ratio for continental China is as small as a few percent [25]. These data are consistent with the results of field experiments carried out at nearly the same time in the United States. For coastal (Delaware Bay) and continental (Bakersfield, CA) regions, it was found that $[Fe(II)]/[Fe]_\Sigma = 0.02$–$0.55$ [26, 27]. For an orographic cloud [33] whose drops contain $(2–3) \times 10^{-7}$ mol/l of iron, the Fe(II) concentration in some samples was below the sensitivity limit of the analytical method. However, these measurements were taken in the nighttime, when the illuminance and, accordingly, $[HO^{\cdot}_{2(g)}]$ were vanishingly low.

Here, it is pertinent to remark that making a comparison between field $[Fe(II)]/[Fe]_\Sigma$ data presented here or known from other sources and the results of numerical simulation in the RM framework is obviously the roughest approximation. This is due to the fact that uncontrollable air influx into the cloud from the environment and variable concentration conditions, temperature, insolation conditions, etc. are inherent in field experiments. The experiments discussed here provided no information concerning the fractional makeup of the water drops collected. Nevertheless, based on the inferences made in this study, it is possible to self-consistently interpret a variety of observed manifestations of the redox properties of Fe(III)/Fe(II) in atmospheric water drops. We compared our simulated data with the results of a representative series of experiments in which the distribution of iron ions between their valence states was investigated in fog and cirrus cloud drops [26, 27].[4] In a series of runs at similar illuminances, as the peroxide concentration rose from 1.5×10^{-6} to 78.6×10^{-6} mol/l, there was no equally great rise in ζ, which increased only from ~0.3 to ~0.7. The correlation between the peroxide concentration and ζ is weak because only a small part of the peroxides is consumed in iron(II) oxidation. For the most part they are apparently spent for sulfite oxidation. Therefore, the formation of the oxidizing properties of the drops toward the Fe(III)/Fe(II) ion couple under the experimental conditions examined can be due to other processes. This is indicated by the strong correlation between the concentrations of sulfite and reduced iron ions in the drops (the correlation coefficient is ~0.82). This correlation has been explained in terms of the source of Fe and S being the same [26, 27]; however, the analysis carried out in this study suggests another interpretation. Firstly, the existence of this correlation is evidence that the samples consisted largely of drops with $r_0 > l_{OH}$. The increase of the sulfur dioxide concentration in the gas from 0.1×10^{-9} to 3×10^{-9} mol/m^3 (0.1–3 ppb) makes the consequences of the nonuniform $OH^{\cdot}_{aq}$ distribution in the drop bulk more pronounced. This causes an increase in the reducing capacity of the drop towards the Fe(III)/Fe(II) ion couple, inevitably leading to a buildup of Fe(II). At the same time, the increase in the $SO_{2(g)}$ concentration favors the redox dissolution of the insoluble forms of iron, thereby raising the total iron content of the drop. Indeed, it is reported that the sulfur content and the total iron content are correlated (the correlation coefficient is ~0.87). The correctness of the above view of the formation of the redox properties of the drops is confirmed by the correlation between the Fe(II) and formaldehyde concentrations observed in the experiments discussed (the correlation coefficient is ~0.95). This correlation is due to the weakening of the conjugation of reactions (26A) and (27A) with reaction (30A), which is caused by the loss of sulfate radicals in their reaction with $HCOO^-_{aq}$. Our calculations for the effect of formaldehyde (1 ppb) on the ratio of oxidized and reduced iron ions in micron-sized drops (see above) led to $\zeta/\zeta_{CH_2O} \approx 3$. A similar situation is observed in the experiments indicating a correlation between Fe(II) and $CH_3CO^-_{2(aq)}$ (the correlation coefficient is ~0.81). It is also possible to explain the seemingly surprising results of another series of field experiments carried out by the same authors (Bakersfield, CA), who observed that, at low acidity (pH 6) due to local ammonia emissions from agriculture, there is a significant increase in ζ ($[Fe(II)]/[Fe]_0 = 0.02$–0.09). This growth of pH obviously causes an increase in the sulfur dioxide solubility and, accordingly, in [S(IV)], because $[S(IV)] \approx [HSO^-_{3(aq)}]$ under atmospheric conditions. Since $[HSO^-_{3(aq)}] \sim 10^{pH}$, the reaction length for the $OH^{\cdot}_{aq}$ radical decreases with increasing pH: $l_{OH} \sim 10^{-pH/2}$. Therefore, the near-surface reactions involving this radical become more significant, enhancing the reducing capacity of the drop towards the Fe(III)/Fe(II) couple. These changes might be expected to cause a buildup of Fe(II). However, one should to take into account the dramatic slowdown of the autocatalytic reaction (6A) and, as a consequence, a marked decrease in the consumption rate of $HSO^-_{5(aq)}$ synthesized in the drop. The

[4] Since most of our calculations refer to pH ≈ 4, it is appropriate to choose measurements made at similar acidities from the totality of data presented in [26, 27]. This requirement is met by samples collected on the Palos Verdes Peninsula (nos. 22–27) and near the Mt. Wilson peak (nos. 28–32). In these experiments, the air temperature, illuminance, and the liquid-water content of the atmospheric air (L) were measured along with determining the chemical composition of samples. Samples 24 and 25 should be excluded from this sample series for the reason that the air did not contain any sulfur dioxide ([S(IV)] ≈ 0) while these samples were pumped through the collector. All samples to be analyzed were collected in the daytime. The water-drop content of the air varied in the $(4–9) \times 10^{-8}$ range, and the acidity of samples ranged between pH 3.6 and 4.2. The iron content of the drops measured by the plasma ionization method, including insoluble iron forms, was $(1.5–9.2) \times 10^{-6}$ mol/l. The concentration of peroxides, including organic peroxides, was $(1.5–78) \times 10^{-6}$ mol/l, and the sulfite content of the drops varied between 1.9×10^{-6} and 17.8×10^{-6} mol/l. This very high sulfite concentration is due to the presence of ammonia in the atmosphere ($(6.3–7) \times 10^{-4}$ mol/l in samples 28, 29, and 32).

rate of reaction (30A) increases under these conditions, causing an increase in the extent of conjugation of this reaction with reactions (26A) and (27A). This greatly enhances the oxidizing capacity of the drop toward iron ions. This effect overbalances the negative effect of the nonuniform $OH^{\bullet}_{aq}$ distribution in the drop, resulting finally in the observed buildup of Fe(III).

ACKNOWLEDGMENTS

This study was supported by the Presidium of the Russian Academy of Sciences through program no. 16, "Changes in the Environment and Climate—Natural Disasters."

REFERENCES

1. Hoffman, M.R. and Jacob, D., in *SO_2, NO, and NO_2 Oxidation Mechanisms: Atmospheric Considerations*, Calvert, J.G., Ed., Boston: Butterworth, 1984, p. 101.
2. Graedel, T.E., Mandlich, M.L., Weshler, S.J., et al., *J. Geophys. Res.*, 1986, vol. 91, p. 5205.
3. Warneck, P., *Chemistry of the Natural Atmosphere*, London: Academic, 2000, p. 927.
4. Brandt, C. and van Eldik, R., *Chem. Rev.*, 1995, vol. 95, no. 1, p. 119.
5. Yermakov, A.N. and Purmal, A.P., *Prog. React. Kinet. Mech.*, 2003, vol. 28, no. 3, p. 189.
6. Travina, O.A., Kozlov, Yu.N., Purmal', A.P., et al., *Zh. Fiz. Khim.*, 1999, vol. 73, p. 1361 [*Russ. J. Phys. Chem.* (Engl. Transl.), vol. 73, p. 1215].
7. Ibusuki, T. and Barnes, H.M., *Atmos. Environ.*, 1984, vol. 18, p. 145.
8. Ibusuki, T. and Takeuchi, K., *Atmos. Environ.*, 1987, vol. 21, p. 1555.
9. Berglund, J., Fronaeous, S., and Elding, L.I., *Atmos. Environ.*, 1995, vol. 29, no. 12, p. 1379.
10. Podkrajsek, B. and Bercic, G., Tursic, et al., *J. Atmos. Chem.*, 2004, vol. 47, p. 283.
11. Ermakov, A.N., Larin, I.K., Ugarov, A.A., and Purmal', A.P., *Kinet. Katal.*, 2003, vol. 44, no. 4, p. 524 [*Kinet. Catal.* (Engl. Transl.), vol. 44, no. 4, p. 476].
12. Cox, P.A., *The Elements on Earth: Inorganic Chemistry in the Environment*, Oxford: Oxford Univ. Press, 1995, p. 255.
13. Latimer, W., *Oxidation Potentials*, New York: Prentice-Hall, 1952, p. 392.
14. Hong, H. and Kester, D.R., *Limnol. Oceanogr.*, 1986, vol. 31, p. 512.
15. Landing, W.M. and Westerlund, S., *Mar. Chem.*, 1988, vol. 23, p. 3219.
16. McKnight, D.M., Kimball, B.A., and Bencala, K.E., *Science*, 1988, vol. 240, p. 637.
17. Hansen, L.D., Silbermann, D., Fisher, G.L., et al., *Environ. Sci. Technol.*, 1984, vol. 18, p. 181.
18. Martin, J.H. and Fitzwater, S.E., *Nature*, 1988, vol. 331, p. 341.
19. Chisholm, S.W. and Morel, F.M.M., *Limnol. Oceanogr.*, 1991, vol. 36, p. 1.
20. Jackson, G.A. and Morgan, J.J., *Limnol. Oceanogr.*, 1978, vol. 230, p. 268.
21. Ermakov, A.N., Larin, I.K., Ugarov, A.A., and Purmal', A.P., *Kinet. Katal.*, 2006, vol. 47, no. 6, p. 849 [*Kinet. Catal.* (Engl. Transl.), vol. 47, no. 6, p. 812].
22. Herrmann, H., Ervens, B., Jacobi, H.-W., et al., *J. Atmos. Chem.*, 2000, vol. 36, p. 231.
23. Warneck, P. and Ziajka, J., *Ber. Bunsen-Ges Phys. Chem.*, 1995, vol. 9, p. 59.
24. Deguillaume, L., Leriche, M., Monod, A., et al., *Atmos. Chem. Phys. Discuss.*, 2003, vol. 3, p. 5019.
25. Zhuang, G., Zhen, Y., and Duce, R.A., *Nature*, 1992, vol. 355, p. 537.
26. Erel, Y., Pehkonen, S.O., and Hoffmann, M.R., *J. Geophys. Res.*, 1993, vol. 98, p. 18 423.
27. Pehkonen, S.O., Erel, Y., Seifert, R.L., et al., *Israel J. Earth Sci.*, 1994, vol. 43, p. 279.
28. Bal, Reddy K. and van Eldik, R., *Atmos. Environ.*, 1992, vol. 26A, p. 661.
29. Schwartz, S.E. and Freiberg, J.E., *Atmos. Environ.*, 1981, vol. 15, p. 1129.
30. Zhu, X.R., Prospero, J.M., Savoie, D.L., et al., *J. Geophys. Res.*, 1993, vol. 98, p. 9039.
31. Radojevic, M., *Environ. Technol. Lett.*, 1984, vol. 5, p. 549.
32. Behra, P. and Sigg, L., *Nature*, 1990, vol. 344, p. 419.
33. Sedlak, D.L., Hoigne, J., David, M.M., et al., *Atmos. Environ.*, 1997, vol. 31, no. 16, p. 2515.